Supplemental Information: On the importance of a precise crystal structure for simulating gas adsorption in nanoporous materials†

Keith V. Lawler,[a] Zeric Hulvey,[a,b] and Paul M. Forster*[a]

1 Experimental Details

HKUST-1 was synthesized using the procedure of Rowsell et al.[1] For our single gas adsorption isotherms, about 150 mg of HKUST-1 was introduced into a previously calibrated sample tube. By carrying out empty tube calibrations prior to measurements, we eliminate the need for He free space measurements that can limit the accuracy of low pressure points. The samples were activated under dynamic vacuum at 180°C for 24 hours. The experimental mass of the samples was determined by subtracting the mass of the empty sample tube and the mass of the sample tube post activation. Gas adsorption isotherms were measured according to our previously published procedure[2] using a Micromeritics ASAP 2020 instrument fitted with a helium cryostat with a stability of better than ±0.01 K. The isotherms were collected over a pressure range of 0 to ∼710 mmHg from 5 cm^3/g incremental volumetric doses with long equilibration times for each dose. Desorption measurements were taken at the end of each isotherm. Each measurement used here displayed negligible hysteresis, indicating that equilibrium had been achieved and there were no leaks in the system affecting the data. Between each isotherm measurement, the sample was reactivated for at least an hour under dynamic vacuum at 100°C, and then placed in the cryostat for at least an hour prior to the measurement of the isotherm in order to equilibrate the sample to the desired temperature. The first measured isotherm was for N_2 at 77.355K for BET surface area analysis. The BET[3] surface area for this particular sample of HKUST-1 is 1684m^2/g.

2 Simulation Details

The universal force field (UFF)[4] has been used to model all the framework atoms as it has been shown to work well for modeling adsorption in MOFs previously.[5] Previously we used a Kr force field derived from the theorem of corresponding states.[6] The two-parameter principle of corresponding states states that the well-depth scales directly with the critical temperature, $\varepsilon \propto T_c$, and that the collision diameter scales with the cube root of the critical volume, $\sigma \propto V_c^{1/3}$.[6] We have computed a force field for Xe using the same technique and revised the Kr force field with updated critical parameters recently obtained from the latest edition of the CRC.[7] Ar is used here as the reference for the proportionality with its Lennard-Jones parameters taken from Hirschfelder's book.[8] Table 1 contains the determined force field parameters and the critical parameters.

We have noticed that many models that only use 12-6 Lennard-Jones potentials for all of the interactions tend to underestimate loading at pressures where gas-gas interactions become important. Looking back at the pair potentials for Kr and Xe indicates that the condensed phases of these gases are better modeled by a potential with a softer repulsion. To account for this we have chosen to use the very common 9-6

	σ(Å)	ε(K)	T_c(K)	P_c(MPa)	$V_c(\frac{cm^3}{mol})$	KD(Å)
Ar	3.405	119.80	150.687	4.863	75	3.542
Kr	3.632	166.40	209.48	5.525	91	3.655
Xe	3.960	230.30	289.733	5.842	118	4.047

Table 1 Parametrization and Kinetic Diameter (KD)[9] of the noble gas atoms.

Lennard-Jones potential to model the gas-gas interactions using the COMPASS force field parameters for Kr and Xe.[10]

	r_0(Å)	ε(kcal/mol)
Ar	3.88	0.20
Kr	4.30	0.28
Xe	4.26	0.39

Table 2 COMPASS 9-6 Lennard-Jones parameters for the noble gas atoms. r_0 is the location of the well minimum and ε is the well depth.

Each simulation employed 200,000 equilibration cycles and 300,000 production cycles. A cycle here consisted of N moves, where N is the number of adsorbed particles (minimum 20). The adsorbate/framework interactions are modeled with 12-6 Lennard-Jones (LJ) potentials cutoff at 15 Å with atomistic parameters combined using the Lorentz-Berthelot mixing rules. The gas-gas interactions were also cutoff at 15 Å. All simulated isotherms are excess corrected using the volumetric method.[11,12] The pore volume was taken as the average of 20 simulations of 10,000,000 trials of the adsorption second virial coefficient: $B = \frac{1}{m}\int e^{-U(\mathbf{r})/kT} d\mathbf{r} - V^g$. For He at 298K, B is assumed to be 0.

3 Structures

The different HKUST-1 structures are all previously published and in the space group $Fm\bar{3}m$.[2,13] 1999 is the originally published structure that has been manually de-solvated. BM is a bare structure measured at a synchrotron at 140K. ND is a bare structure measured by neutron powder diffraction at 8K. Xe1, Xe2, Xe3, Xe4, and Xe5 are structures with different increasing doses of Xe in the framework measured by synchrotron at 260K, 260K, 260K, 260K, and 240K, respectively. Kr1, Kr2, and Kr3 are structures with different increasing doses of Kr in the framework measured by synchrotron at 200K, 180K, 140K. Ar1 is a structure measured with enough Ar to fill the small pockets by neutron powder diffraction at 8K. The fractional coordinates for each structure (with guest atoms removed) are presented below. The crystallographically unique carbons are labeled as CA (carbonyl), CB (phenyl bound to carbonyl C), CC (phenyl bound to H). Table 3 lists the approximate window diameters for each HKUST-1 structure. The window is most easily defined by a triangle of CC's. The window's radius is determined here by finding the centroid of the three carbons defining the window and determining the distance from the centorid to each CC atom. The radius is modified to reflect the actual accessible volume by subtracting carbon's van der Waals radius (1.70 Å)[7]. The window diameter is found by multiplying the final radius by 2. Due to symmetry, the diameter determined in this fashion is the same regardless of which particular carbon and window is examined. The hydrogen atoms were not used to define the window as their coordinates are difficult to determine experimentally, and they are far more mobile than the carbons.

1999	BM	ND	Ar1	Kr1	Kr2	Kr3	Xe1	Xe2	Xe3	Xe4	Xe5
3.745	3.691	3.651	3.655	3.681	3.505	3.600	3.708	3.678	3.610	3.661	4.000

Table 3 Approximate window diameter (Å) for each of the HKUST-1 structures.

atom	a	b	c
Cu	0.28527(3)	0.28527(3)	0.0000
O	0.31664(14)	0.24313(14)	-0.05224(14)
CB	0.3220(2)	0.1780(2)	-0.1130(3)
CA	0.2968(2)	0.2032(2)	-0.0687(3)
CC	0.3655(2)	0.1994(3)	-0.1345(2)
H	0.3802(2)	0.2280(3)	-0.1198(2)

Table 4 Fractional coordinates for 1999. Lattice parameter is 26.343(5)Å

atom	a	b	c
Cu	0.28380(6)	0.28380(6)	0.0000
O	0.31642(15)	0.24556(17)	-0.05029(14)
CB	0.32133(27)	0.17867(27)	-0.1129(4)
CA	0.29481(27)	0.20519(27)	-0.06780(34)
CC	0.36574(32)	0.2006(4)	-0.13426(32)
H	0.3856(15)	0.2320(19)	-0.1144(15)

Table 5 Fractional coordinates for BM. Lattice parameter is 26.29580(26)Å

atom	a	b	c
Cu	0.28313(11)	0.28313(11)	0.0000
O	0.31708(10)	0.24417(10)	-0.05215(9)
CB	0.32165(9)	0.17835(9)	-0.11333(12)
CA	0.29637(8)	0.20363(8)	-0.06921(12)
CC	0.36476(9)	0.20064(13)	-0.13524(9)
H	0.38109(16)	0.23480(21)	-0.11892(16)

Table 6 Fractional coordinates for ND. Lattice parameter is 26.3067(4)Å

atom	a	b	c
Cu	0.2830(1)	0.2830(1)	0.0000
O	0.31701(8)	0.24373(9)	-0.05228(8)
CB	0.32180(8)	0.17820(8)	-0.1130(1)
CA	0.29634(7)	0.20366(7)	-0.0693(1)
CC	0.36473(7)	0.2004(1)	-0.13527(7)
H	0.3810(1)	0.2350(2)	-0.1190(1)

Table 7 Fractional coordinates for Ar1. Lattice parameter is 26.2919(3)Å

atom	a	b	c
Cu	0.2836(1)	0.2836(1)	0.0000
O	0.3161(2)	0.2464(2)	-0.0502(2)
CB	0.3210(3)	0.1791(3)	-0.1134(4)
CA	0.2948(3)	0.2052(3)	-0.0684(4)
CC	0.3660(3)	0.2011(4)	-0.1340(3)
H	0.382(2)	0.237(2)	-0.118(2)

Table 8 Fractional coordinates for Kr1. Lattice parameter is 26.2928(3)Å

atom	a	b	c
Cu	0.2832(1)	0.2832(1)	0.0000
O	0.3160(2)	0.2451(2)	-0.0501(2)
CB	0.3206(3)	0.1794(3)	-0.1156(4)
CA	0.2958(3)	0.2042(3)	-0.0689(4)
CC	0.3660(4)	0.2052(5)	-0.1340(4)
H	0.389(2)	0.232(4)	-0.111(2)

Table 9 Fractional coordinates for Kr2. Lattice parameter is 26.2945(3)Å

atom	a	b	c
Cu	0.2839(1)	0.2839(1)	0.0000
O	0.3161(2)	0.2456(3)	-0.0498(2
CB	0.3208(4)	0.1792(4)	-0.1137(6)
CA	0.2938(4)	0.2062(4)	-0.0684(5)
CC	0.3650(5)	0.2020(5)	-0.1350(5)
H	0.384(3)	0.234(3)	-0.116(3)

Table 10 Fractional coordinates for Kr3. Lattice parameter is 26.2954(3)Å

atom	a	b	c
Cu	0.2839(1)	0.2839(1)	0.0000
O	0.3162(2)	0.2467(2)	-0.0502(2)
CB	0.3213(3)	0.1787(3)	-0.1135(4)
CA	0.2935(3)	0.2065(3)	-0.0677(4)
CC	0.3661(3)	0.2005(4)	-0.1339(3)
H	0.381(2)	0.239(2)	-0.1200(2)

Table 11 Fractional coordinates for Xe1. Lattice parameter is 26.2874(3)Å

atom	a	b	c
Cu	0.2837(1)	0.2837(1)	0.0000
O	0.3169(2)	0.2451(2)	-0.0506(2)
CB	0.3203(3)	0.1797(3)	-0.1129(4)
CA	0.2919(3)	0.2082(3)	-0.0694(4)
CC	0.3665(3)	0.2016(4)	-0.1335(3)
H	0.388(2)	0.231(2)	-0.112(2)

Table 12 Fractional coordinates for Xe2. Lattice parameter is 26.2872(3)Å

atom	a	b	c
Cu	0.2837(1)	0.2837(1)	0.0000
O	0.3156(2)	0.2462(2)	-0.0497(2)
CB	0.3213(3)	0.1787(3)	-0.1138(5)
CA	0.2930(3)	0.2070(3)	-0.0692(4)
CC	0.3667(4)	0.2034(5)	-0.1333(4)
H	0.389(2)	0.231(3)	-0.111(2)

Table 13 Fractional coordinates for Xe3. Lattice parameter is 26.2868(3)Å

atom	a	b	c
Cu	0.2836(1)	0.2836(1)	0.0000
O	0.3145(2)	0.2467(2)	-0.0498(2)
CB	0.3209(3)	0.1791(3)	-0.1138(4)
CA	0.2943(3)	0.2057(3)	-0.0690(4)
CC	0.3668(4)	0.2023(5)	-0.1332(4)
H	0.388(1)	0.232(2)	-0.112(1)

Table 14 Fractional coordinates for Xe4. Lattice parameter is 26.2867(3)Å

atom	a	b	c
Cu	0.2833(1)	0.2833(1)	0.0000
O	0.3142(2)	0.2471(2)	-0.0505(2)
CB	0.3217(3)	0.1783(3)	-0.1120(4)
CA	0.2934(2)	0.2066(2)	-0.0694(4)
CC	0.3701(3)	0.1977(5)	-0.1299(3)
H	0.3869(3)	0.2324(6)	-0.1131(3)

Table 15 Fractional coordinates for Xe5. Lattice parameter is 26.2886(4)Å

	1999	BM	ND	Ar1	Kr1	Kr2	Kr3	Xe1	Xe2	Xe3	Xe4	Xe5
pocket	0.000	0.000	0.000	0.26	0.112	0.175	0.242	0.432	0.670	0.757	0.799	0.930
window	0.000	0.000	0.000	0.000	0.000	0.100	0.316	0.000	0.072	0.091	0.111	0.240

Table 16 Crystallographically determined site occupancies for respective noble gas in each of the structures.

4 Comparing Gas-Gas Force Fields

Here we present the comparisons of using a 12-6 Lennard-Jones potential versus a 9-6 Lennard-Jones potential to model the gas-gas interactions. The 12-6 Lennard-Jones potential used the same atomistic parameters for Kr and Xe as shown in table 1 that were used to construct the gas-framework interaction.

When using only a 12-6 Lennard-Jones force field for gas adsorption in MOFs and zeolites, it can generally be observed that the initial agreement with most MOF force fields is very good initially. However as the loading increases and gas-gas interactions become more important, the simulated isotherms tend to go asymptotic at too low of a total loading than is measured experimentally. We observe this most frequently with Xe at the temperatures we typically measure isotherms 250-300K, for example figure 4. We have observed this not just for HKUST-1 but in other materials such as zeolites. By looking back at the predicted pair potentials for condensed Kr and Xe, it can be seen that a 12-6 Lennard-Jones potential is not particularly ideal for predicting the properties of Kr and Xe, and Kr and Xe pair potentials tend to be better modeled with a softer repulsion term.[14–16] The 9-6 Lennard-Jones potential is very common in molecular mechanics, and it intrinsically provides the softer repulsion needed for the problem. The use of a 9-6 potential for gas-gas interaction immediately fixed this lower asymptotic value for Xe (fig. 3). The same problem is observed with the Kr isotherms, but not to the same extant. First, the derived pair potential using 12-6 potentials do actually have better agreement with Kr than with Xe, indicating that while not ideal a 12-6 potential provides a reasonable description of the interactions occurring in Kr as it condenses. Secondly, our measured Kr isotherms are still increasing fairly linearly at our imposed instrument limit of $\sim$700 torr. We are likely not as far into the loading regime where gas-gas interactions really matter like we are at our largest measured isotherm point for Xe, therefore the shift to a 9-6 potential will be less noticeable. We have also included comparisons of the mean absolute percent error of each simulated isotherm in each force field compared to experiment in tables 17 and 18. While the 12-6 MAPE looks deceivingly good, it is only because we were not able to take experimental measurements beyond 1 bar. Had the data-set extended that far, the numbers would be far more shocking as is visibly apparent by how the curvatures of all the simulated isotherms do not well match that of the experimental isotherms.

	1999	BM	ND	Ar1	Kr1	Kr2	Kr3	Xe1	Xe2	Xe3	Xe4	Xe5
Kr	16.3	11.7	3.7	3.8	4.5	3.3	4.8	9.5	15.3	9.4	11.1	25.6
Xe	3.2	5.9	15.6	15.3	19.7	10.1	11.5	24.1	3.2	6.2	6.3	4.8

Table 17 Mean absolute percent error agreement of simulated isotherm to experimental isotherm. Gas-gas interactions are done with a 9-6 Lennard-Jones potential.

	1999	BM	ND	Ar1	Kr1	Kr2	Kr3	Xe1	Xe2	Xe3	Xe4	Xe5
Kr	12.0	8.1	6.8	6.3	8.3	7.3	5.1	12.1	9.7	5.3	6.9	21.2
Xe	5.5	5.2	14.3	14.1	18.4	8.3	10.0	23.0	3.5	4.8	5.2	3.4

Table 18 Mean absolute percent error agreement of simulated isotherm to experimental isotherm. Gas-gas interactions are done with a 12-6 Lennard-Jones potential.

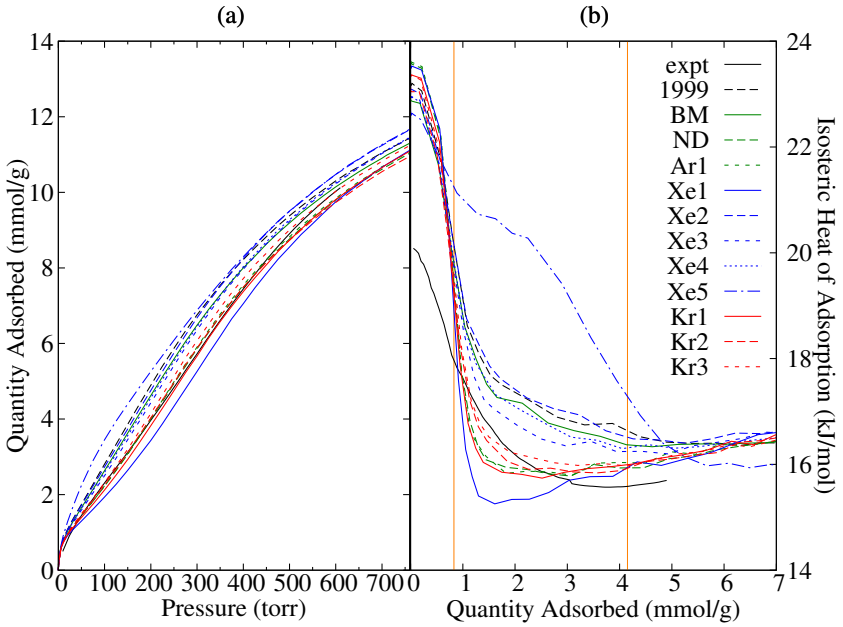

Fig. 1 Simulated isotherms (a) and heats of adsorption (b) for Kr at 200K into several different structures of HKUST-1. Vertical lines represent a sufficient gas loading to saturate the center, and the center plus windows of the small pockets. Gas-gas interactions are done with a 9-6 Lennard-Jones potential.

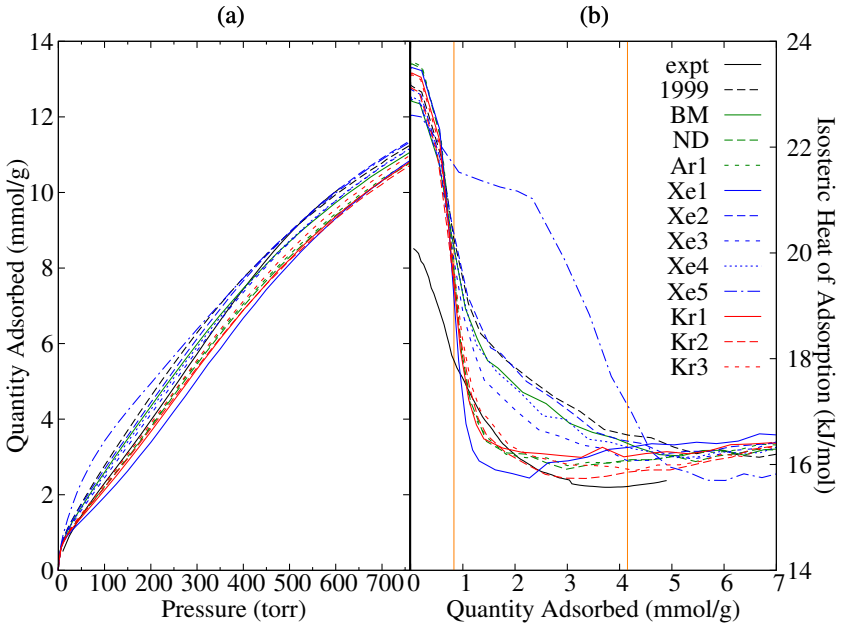

Fig. 2 Simulated isotherms (a) and heats of adsorption (b) for Kr at 200K into several different structures of HKUST-1. Vertical lines represent a sufficient gas loading to saturate the center, and the center plus windows of the small pockets. Gas-gas interactions are done with a 12-6 Lennard-Jones potential.

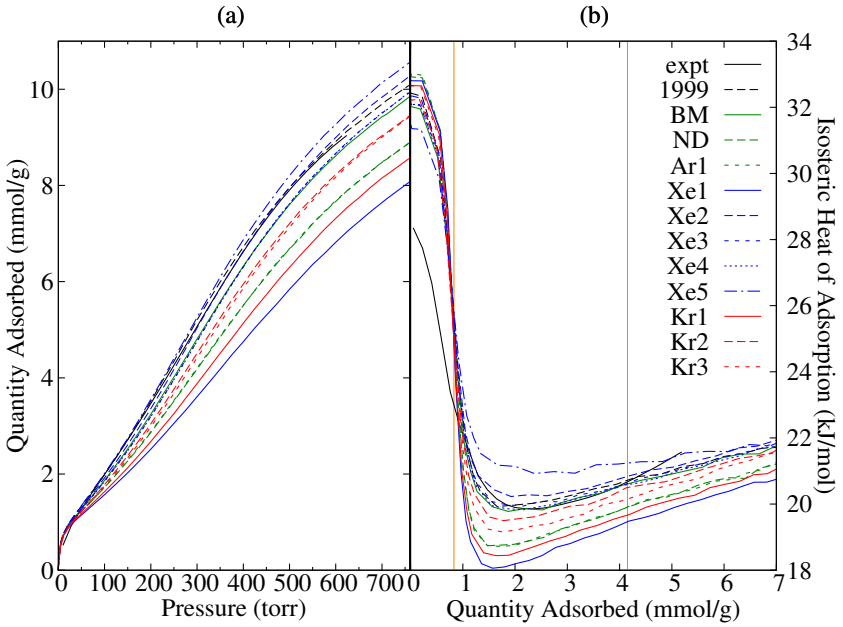

Fig. 3 Simulated isotherms (a) and heats of adsorption (b) for Xe at 260K into several different structures of HKUST-1. Vertical lines represent a sufficient gas loading to saturate the center, and the center plus windows of the small pockets. Gas-gas interactions are done with a 9-6 Lennard-Jones potential.

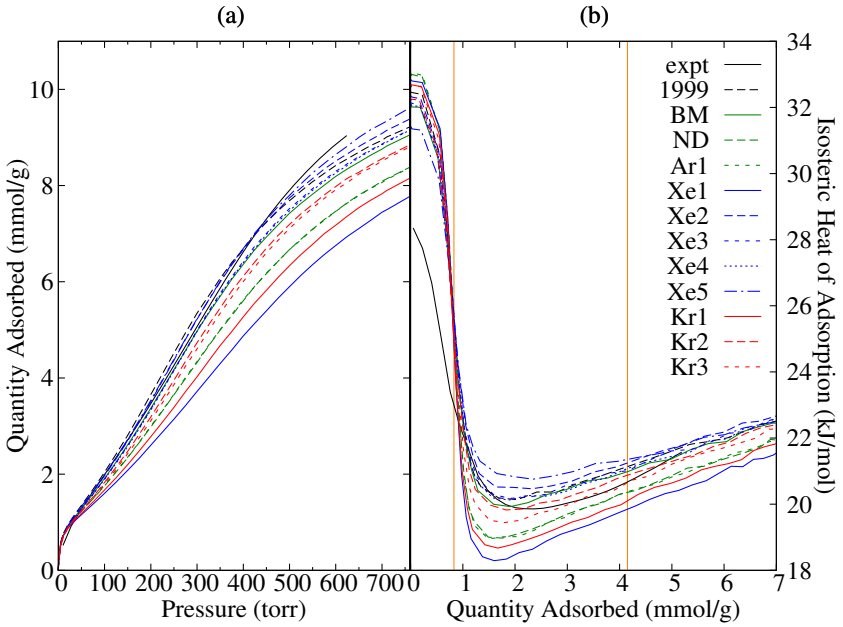

Fig. 4 Simulated isotherms (a) and heats of adsorption (b) for Xe at 260K into several different structures of HKUST-1. Vertical lines represent a sufficient gas loading to saturate the center, and the center plus windows of the small pockets. Gas-gas interactions are done with a 12-6 Lennard-Jones potential.

5 Potential Energy Surfaces for HKUST-1

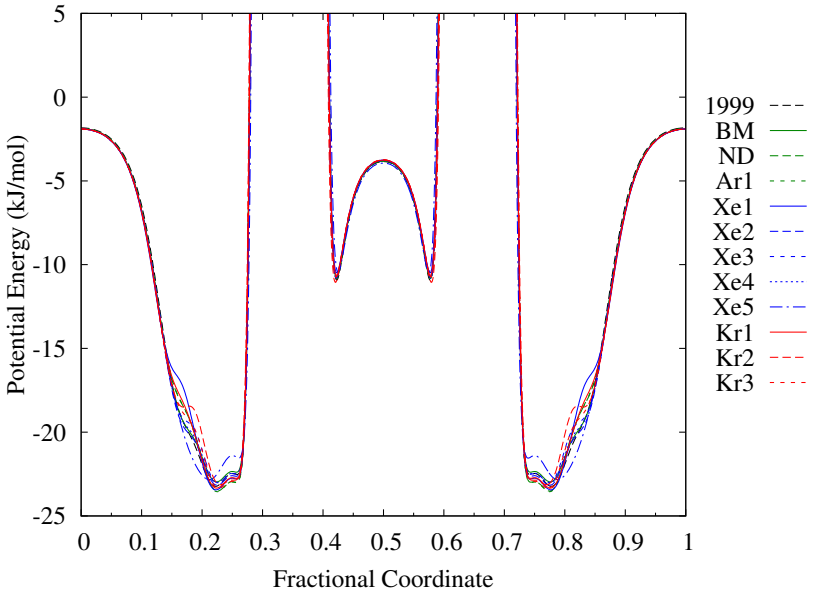

Fig. 5 The potential energy for a Kr atom along the 3-fold axis from (0,0,0) to (1,1,1) in steps of 1/1000 of a fractional coordinate.

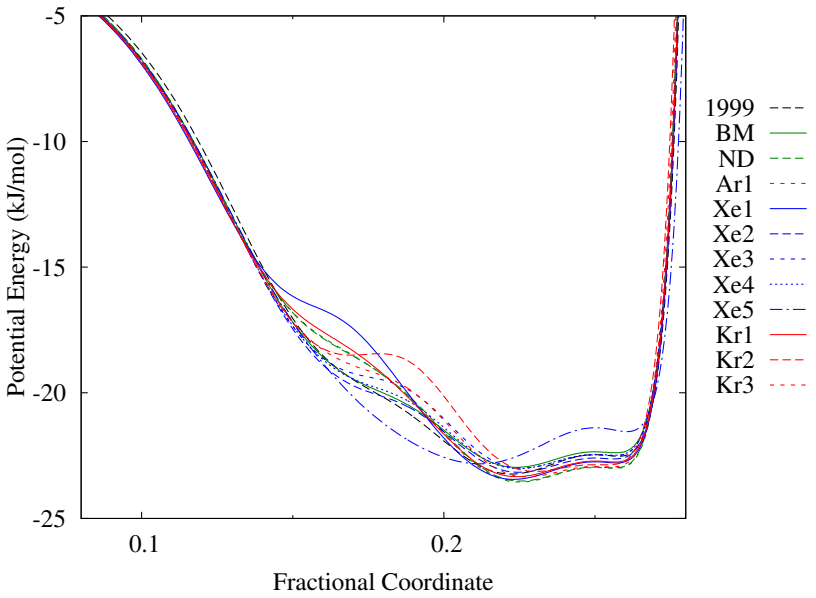

Fig. 6 The potential energy for a Kr atom along the 3-fold axis from (0.08,0.08,0.08) to (0.30,0.30,0.30) in steps of 1/1000 of a fractional coordinate.

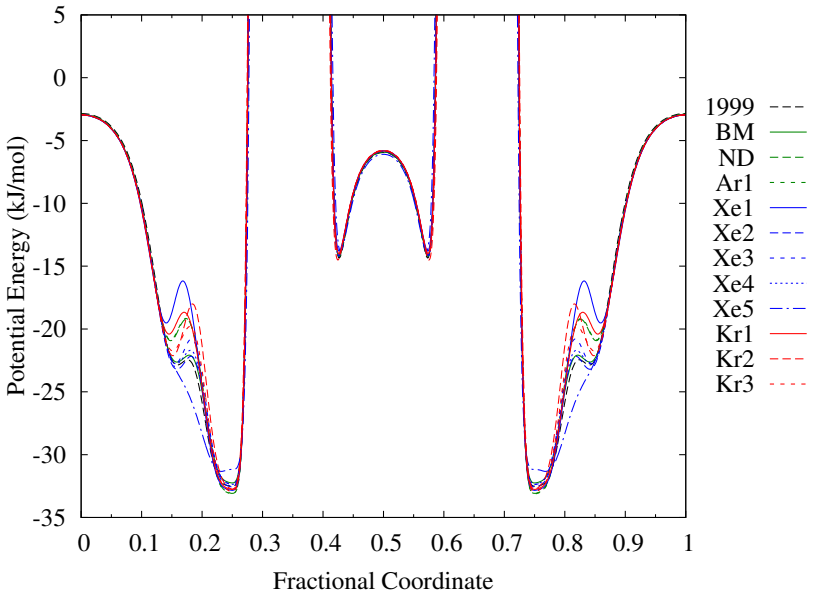

Fig. 7 The potential energy for a Xe atom along the 3-fold axis from (0,0,0) to (1,1,1) in steps of 1/1000 of a fractional coordinate.

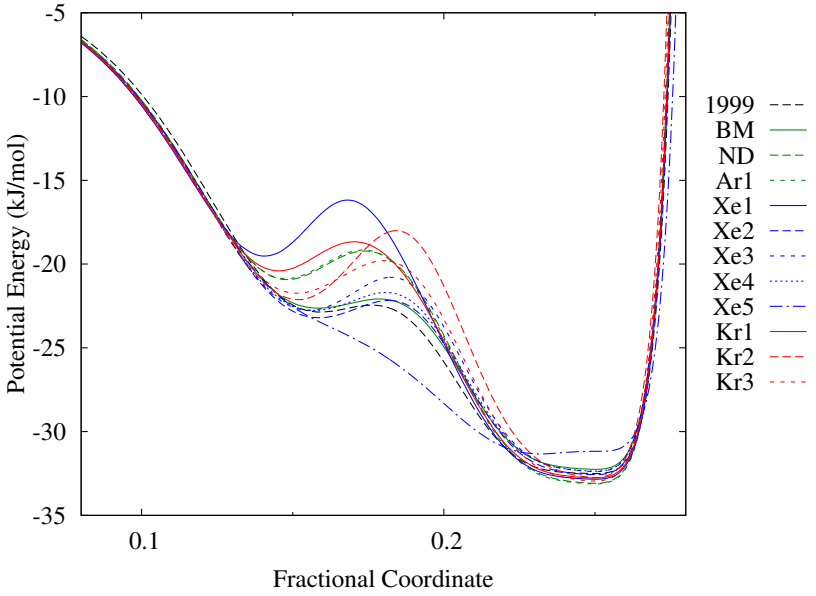

Fig. 8 The potential energy for a Xe atom along the 3-fold axis from (0.08,0.08,0.08) to (0.30,0.30,0.30) in steps of 1/1000 of a fractional coordinate.

6 Calculations with Dipole Polarization

To verify the extent of the participation of the open metal site we modified our energetics to include dipole polarization ($U_{pol}=-\frac{1}{2}\alpha|\vec{E}|^2$).[17] As the noble gases are non-polar and have no standing multipole moment, dipole polarization is the leading electrostatic term for their interaction with a charged open metal site. The HKUST-1 partial charges were taken from a previous work that used the CHELPG method to discern the atomic partial charges from accurate quantum mechanical calculations on the Cu paddle-wheel unit.[18–20] The partial charges are Cu +1.00e, O -0.60e, CA 0.70e, CB 0.00e, CC -0.15e, and H 0.15e. The electric field was computed using an Ewald summation. The polarizability volumes for Kr and Xe used here are 2.4844 Å^3 and 4.044 Å^3, respectively.[9] Figures 9 and 10 compare the isotherms and heats of adsorptions found with (blue) and without (red) dipole polarization for Kr/Xe into the the best Kr adsorbing structure "Kr2". The figures clearly show there is little difference in the predicted adsorption properties when dipole polarization is included, and the numerical values differ by around 1%. The total energetics from the dipole polarization is 300-fold less than the Xe-HKUST-1 interaction at 1 atmosphere and 10000-fold less around 1 torr. Likewise, the total energetics from the dipole polarization is 250-fold less than the Kr-HKUST-1 interaction at 1 atmosphere and 10000-fold less around 1 torr. This energetic discrepancy explains why there is little noticeable difference between the simulations. The electrostatic interactions at the open metal sites are not sufficient to make them the energetically preferred binding site over the center of the small pockets or the windows into the pockets. Some test calculations show us that a charge like that on Cu should be enough to reasonably polarize Xe, however it is our hypothesis that the nearby oxygen atoms shield some of the electric field emanating from the Cu and lowers the overall effect of the dipole polarization of the noble gases.

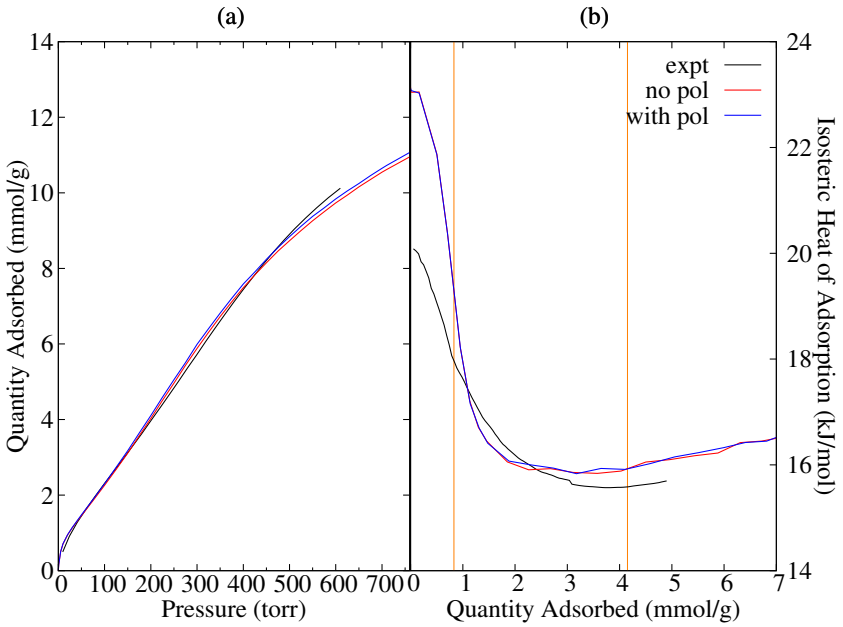

Fig. 9 Simulated isotherms (a) and heats of adsorption (b) for Kr at 200K into the best Kr adsorbing structure "Kr2" both with (blue) and without (red) dipole polarization for Kr. Gas-gas interactions are done with a 9-6 Lennard-Jones potential. Vertical lines represent a sufficient gas loading to saturate the center, and the center plus windows in the small pockets.

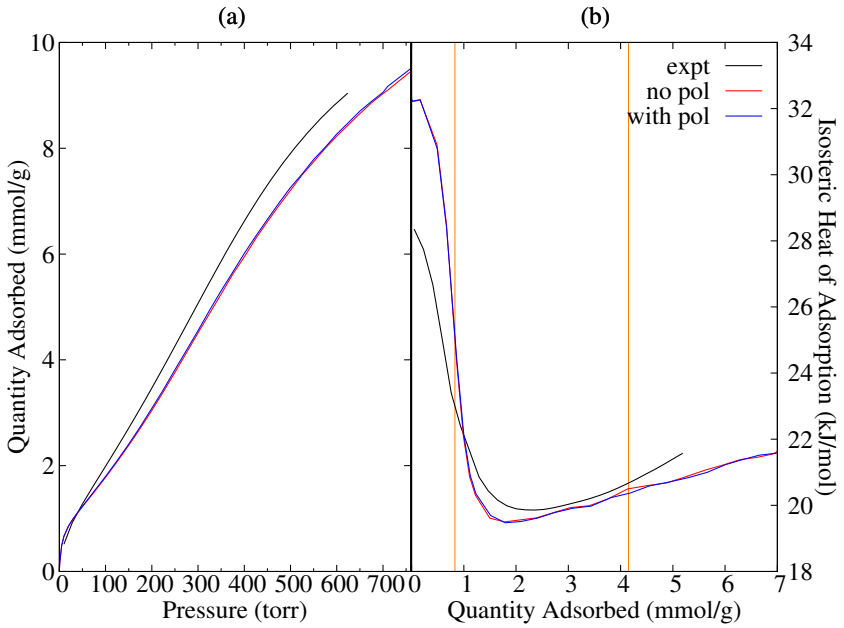

Fig. 10 Simulated isotherms (a) and heats of adsorption (b) for Xe at 260K into the best Kr adsorbing structure "Kr2" both with (blue) and without (red) dipole polarization for Xe. Gas-gas interactions are done with a 9-6 Lennard-Jones potential. Vertical lines represent a sufficient gas loading to saturate the center, and the center plus windows in the small pockets.

7 Calculations incorporating some degree of framework flexibility

A common way of dealing with flexibility in frameworks is to allow the cell to breathe, ie. expand or contract while keeping the atomic fractional positions fixed. To test if this perturbation is sufficient to improve the estimated adsorption, we constructed a hypothetical structure for HKUST-1 (Hyp) using the fractional coordinates of originally reported solvated structure (1999) and the lattice constant of the structure that performed the best for Kr adsorption (Kr2). The change in lattice constant shifted the Cartesian coordinate of the point (1,1,1) inwards by 0.084 Å. Figure 11 shows that the predicted adsorption properties (both Kr and Xe) for the slightly compressed version of "1999" differed by less than 1% from those of the original structure, thus indicating that the differences in the simulated adsorption properties stem predominantly from changes in the HKUST-1 framework rather than the cell volume.

To further test the importance of internal flexibility, NVT molecular dynamics (MD) simulations were performed for various loadings of Kr and Xe into the isovolumic structures "Kr2" and "1999" compressed to have the same lattice constant as "Kr2". The MD simulations were performed with GULP.[21] Although there are many good force fields for the intramolecular interaction in HKUST-1, we opted to use the UFF4MOF to complement the use of UFF for intermolecular interactions.[22] The MD was done without any symmetry, and the integrator used was leapfrog Verlet with a GULP formatted Nose-Hoover weight of 0.10. The Kr loaded cells had a simulation temperature of 200K, and the Xe loaded cells had a simulation temperature of 260K. For the MD the intermolecular potentials were cutoff at 12 Å and a polynomial taper was employed for after 10 Å. The MD simulations had a time step of 1 femtosecond, and were equilibrated for 100 picoseconds. Snapshots of the structure were taken every 100 femtoseconds for at least 500 picoseconds after equilibration. The average structure was computed by averaging the framework atomic positions from every snapshot taken. The window diameters were determined in a similar fashion as the original

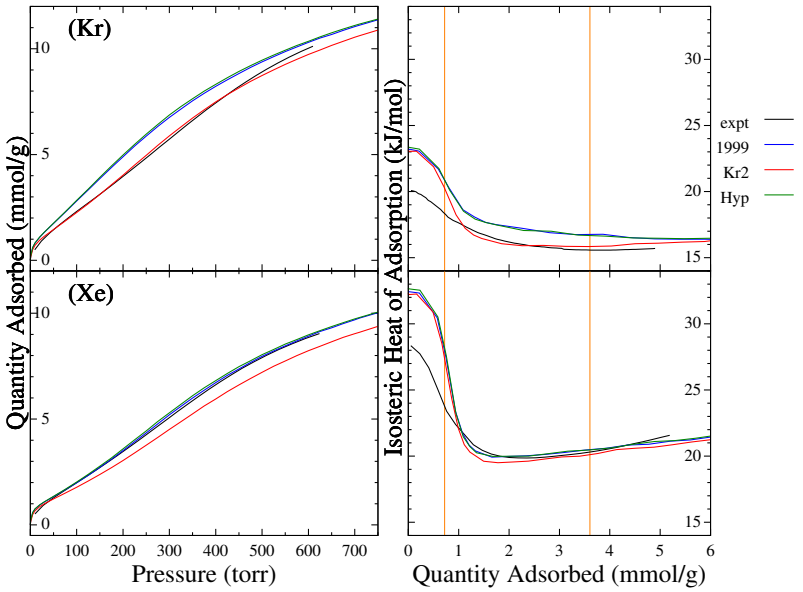

Fig. 11 Simulated isotherms (left) and heats of adsorption (right) for Kr at 200K (top) and Xe at 260K (bottom) into the original de-solvated structure "1999" (blue), the best Kr adsorbing structure "Kr2" (red), and "Hyp" (green) which is a compressed version of "1999" having the same lattice constant as "Kr2". Vertical lines represent a sufficient gas loading to saturate the center, and the center plus windows in the small pockets.

12 structures. The MD snapshots do not obey the $Fm\bar{3}m$ symmetry of the original cells, so the window diameter was determined by first finding the average lattice site for each framework atom, computing the diameter for each centroid-CC combination within the simulation volume of the average structure, and finally those diameters were averaged to obtain the values presented in the main text.

The MD was not done in the full cubic cell, instead the F-centered cell was transformed to the primitive cell in order to reduce the computational effort at least four-fold. The primitive cell has 2 small pockets and one of each of the two large cells. We used 5 initial guesses for Kr and Xe loading into each of the two base structures. The initial loading labeled 'bare' is just the HKUST-1 structure with no gas atoms present, and it was simulated at both 200K and 260K. The initial loading labeled 'pocket' has 2 Kr/Xe atoms, one at the center of each small pocket. This loading should represent the orange line in each HOA plot around 0.8 mmol/g. The initial loading labeled 'p+$\frac{1}{2}$w' has the same atoms as 'pocket' and 4 additional Kr/Xe atoms; the additional atoms occupy 2 of 4 of the window sites of both small pockets. The initial loading labeled 'p+w' has the same atoms as 'pocket' and 8 additional Kr/Xe atoms; the additional atoms occupy each of the window sites of both small pockets. This loading should represent the orange line in each HOA plot around 4.1 mmol/g. The initial loading labeled 'full' has the same atoms as 'p+w' and 10 additional Kr/Xe atoms; the additional atoms are placed at coordinates in the large cells taken at random from the final configuration of the GCMC run for Kr into "Kr2" at 200K and 1 atm.

8 Higher Temperature Isotherms

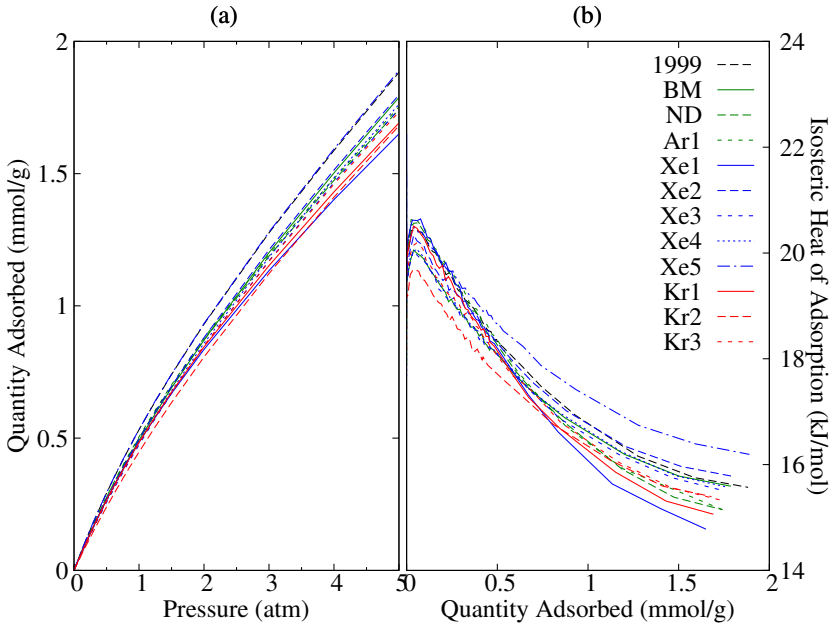

Fig. 12 Simulated isotherms (a) and heats of adsorption (b) for Kr at 350K into several different structures of HKUST-1. Gas-gas interactions are done with a 9-6 Lennard-Jones potential.

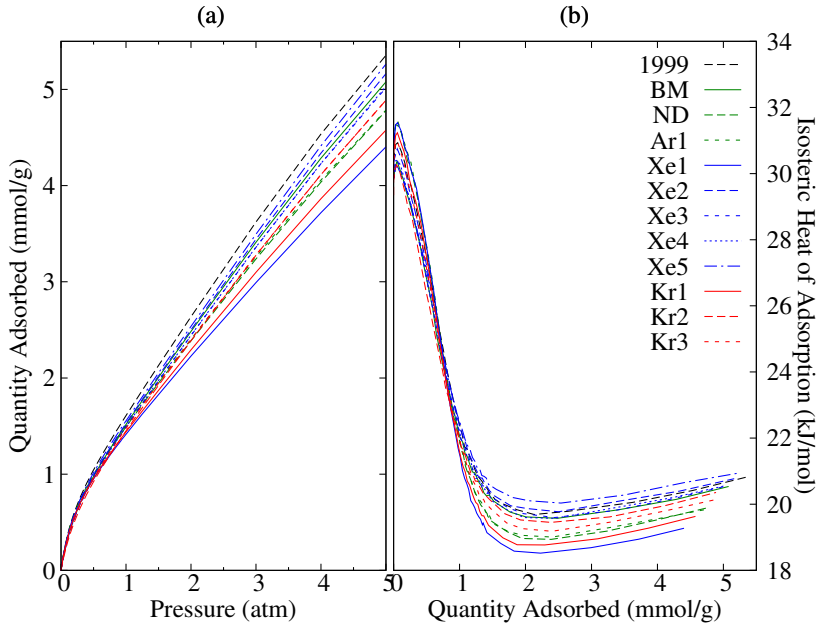

Fig. 13 Simulated isotherms (a) and heats of adsorption (b) for Xe at 350K into several different structures of HKUST-1. Gas-gas interactions are done with a 9-6 Lennard-Jones potential.

References

1 J. L. C. Rowsell and O. M. Yaghi, *J. Am. Chem. Soc.*, 2006, **128**, 1304–1315.
2 Z. Hulvey, K. V. Lawler, Z. Qiao, J. Zhou, D. Fairen-Jimenez, R. Q. Snurr, S. V. Ushakov, A. Navrotsky, C. M. Brown and P. M. Forster, *J. Phys. Chem. C*, 2013, **117**, 20116–20126.
3 S. Brunauer, P. H. Emmett and E. Teller, *J. Am. Chem. Soc.*, 1938, **60**, 309.
4 A. Rappe, C. Casewit, K. Colwell, W. Goddard and W. Skiff, *J. Am. Chem. Soc.*, 1992, **114**, 10024–10035.
5 J. J. Perry, IV, S. L. Teich-McGoldrick, S. T. Meek, J. A. Greathouse, M. Haranczyk and M. D. Allendorf, *J. Phys. Chem. C*, 2014, **118**, 11685–11698.
6 O. Talu and A. Myers, *Colloids Surf., A*, 2001, **187**, 83–93.
7 *CRC Handbook of Chemistry and Physics, 95th ed, 2014-2015*, `http://www.hbcpnetbase.com`.
8 J. O. Hirschfelder, C. F. Curtiss and R. B. Bird, *Molecular Theory of Gases and Liquids*, John Wiley & Sons, Inc., 1954.
9 J.-R. Li, R. J. Kuppler and H.-C. Zhou, *Chem. Soc. Rev.*, 2009, **38**, 1477–1504.
10 J. Yang, A.-M. Tian and H. Sun, *J. Phys. Chem. B*, 2000, **104**, 4951–4957.
11 F. Karavias and A. Myers, *Langmuir*, 1991, **7**, 3118–3126.
12 A. Myers and P. Monson, *Langmuir*, 2002, **18**, 10261–10273.
13 S. Chui, S. Lo, J. Charmant, A. Orpen and I. Williams, *Science*, 1999, **283**, 1148–1150.
14 E. Whalley and W. Schneider, *J. Chem. Phys.*, 1955, **23**, 1644–1650.
15 I. J. Zucker, *Il Nuovo Cimento B Series 10*, 1968, **54**, 177–190.
16 D. W. Gough, E. B. Smith and G. C. Maitland, *Mol. Phys.*, 1974, **27**, 867–872.
17 H. Yu and W. F. van Gunsteren, *Comput. Phys. Commun.*, 2005, **172**, 69–85.
18 C. M. Breneman and K. B. Wiberg, *J. Comput. Chem.*, 1990, **11**, 361.
19 D. Farrusseng, C. Daniel, C. Gaudillere, U. Ravon, Y. Schuurman, C. Mirodatos, D. Dubbeldam, H. Frost and R. Q. Snurr, *Langmuir*, 2009, **25**, 7383–7388.
20 E. García-Pérez, J. Gascón, V. Morales-Flórez, J. M. Castillo, F. Kapteijn and S. Calero, *Langmuir*, 2009, **25**, 1725–1731.
21 J. D. Gale and A. L. Rohl, *Mol. Simul.*, 2003, **29**, 291–341.
22 M. A. Addicoat, N. Vankova, I. F. Akter and T. Heine, *J. Chem. Theory Comput.*, 2014, **10**, 880–891.